


PtP₂: An example of exploring the hidden Cairo tessellation in the pyrite structure for discovering novel two-dimensional materials

Lei Liu and Houlong L. Zhuang*

School for Engineering of Matter Transport and Energy, Arizona State University, Tempe, Arizona 85287, USA

 (Received 9 August 2018; revised manuscript received 20 September 2018; published 6 November 2018)

The Cairo tessellation refers to a pattern of type 2 pentagons that can tile an infinite plane without creating a gap or overlap. We reveal the hidden, layered Cairo tessellations in the pyrite structure with a general chemical formula AB_2 and space group $pa\bar{3}$. We use this hidden tessellation along with density functional theory calculations to examine the possibility of obtaining a two-dimensional (2D) material with the Cairo tessellation from the bulk, using PtP₂ as an example. Unlike previously reported single-layer materials such as PdSe₂ with a buckled, pentagonal structure—strictly speaking, not belonging to the Cairo tessellation, we find that single-layer PtP₂ is completely planar exhibiting dynamically stable phonon modes. We also observe a reduction in the band gaps of PtP₂ from bulk to single layer using the Heyd-Scuseria-Ernzerhof (HSE) hybrid density functional, and the band gap type switches from indirect to direct. By contrast, using the standard Perdew-Burke-Ernzerhof functional leads to the conclusion of single-layer PtP₂ being metallic. We further study the bonding characteristics of this novel single-layer material by computing the Bader charge transfer, the electron localization function, and the crystal orbit overlap population, which show mixed P-P covalent bonding and Pt-P ionic bonding, with the former being stronger. Finally, we study the surface states of single-layer PtP₂ and consider the spin-orbit coupling. We observe no spin-helical Dirac cone states, therefore ruling out single-layer PtP₂ as a topological insulator. We expect the example demonstrated in this work will stimulate interest in computationally identifying novel 2D materials from a variety of bulk materials with the pyrite structure.

DOI: [10.1103/PhysRevMaterials.2.114003](https://doi.org/10.1103/PhysRevMaterials.2.114003)

I. INTRODUCTION

Hexagon is arguably the most favorable geometry adopted by a number of existing two-dimensional (2D) materials such as single-layer graphene [1], boron nitride [2], molybdenum sulfide [3], and chromium tri-iodide [4] that exhibit exotic electrical and magnetic properties. As a result of this popularity, a number of 2D materials predicted by density functional theory (DFT) calculations are assumed to adopt hexagonal structures [5,6].

Pentagon, despite its equal simplicity and beauty, had been a headache for a crystallographer who prefers structures with translational periodicity. However, Shechtman *et al.* accidentally came upon an Al-Mn alloy with a pentagonal structure [7]. This alloy is still called a crystal but with a prefix “quasi” because of its “long-range orientational order and no translational symmetry.”

To remove this unpleasant prefix, we recently spent efforts in coupling pentagonal geometries with DFT calculations to predict new 2D crystalline materials. We started with placing atoms of an element at the vertices of the newly discovered type 15 pentagons. We tested eight elements, but we found that no element can form a nanosheet of type 15 pentagons after DFT geometry optimizations [8]. We then focused on using only one element, carbon, and locate its atoms at the vertices of the other 14 types of pentagons [9]. We found

that the carbon nanosheet made of type 2 pentagons remained the same as the initial input type of pentagonal structure. Interestingly, the carbon nanosheet based on type 4 pentagons was optimized into the same structure as resulted from type 2 pentagons. By contrast, the carbon nanosheets built upon the other 12 types of pentagons cannot retain their pentagonal structures. These previous calculations indicate that type 2 pentagon is the most promising pentagon that can be used to discover new 2D materials.

Type 2 pentagon is one of the existing 15 types of irregular, convex pentagons discovered so far that can tile a plane without rendering any overlap or gap [10]. The topology of this type of pentagon is not unique, because there are only two constraints on the side lengths c and e ($c = e$) and on the angles B and D ($B + D = 180^\circ$), leaving three degrees of freedom. The pentagon illustrated in Fig. 1(a) is a special topology of type 2 pentagon with two additional geometry constraints: $b = c = d = e$ and $B = D = 90^\circ$. The tiling of this special topology leads to the so-called Cairo tessellation, a pattern that gains its name, as it is ubiquitous on the streets of Cairo in Egypt [11].

Pentagonal structures with the Cairo tessellation can be straightforwardly identified in van der Waals layered materials such as PdSe₂. Each layer of PdSe₂ consists of Pd and Se atoms located at the vertices of type 2 pentagons. Note that these atoms are not settled in the same plane. As a result of the weak van der Waals forces, single-layer PdSe₂ has been successfully exfoliated from its bulk counterpart with the mechanical exfoliation method, exhibiting a band gap

*zhuanghl@asu.edu

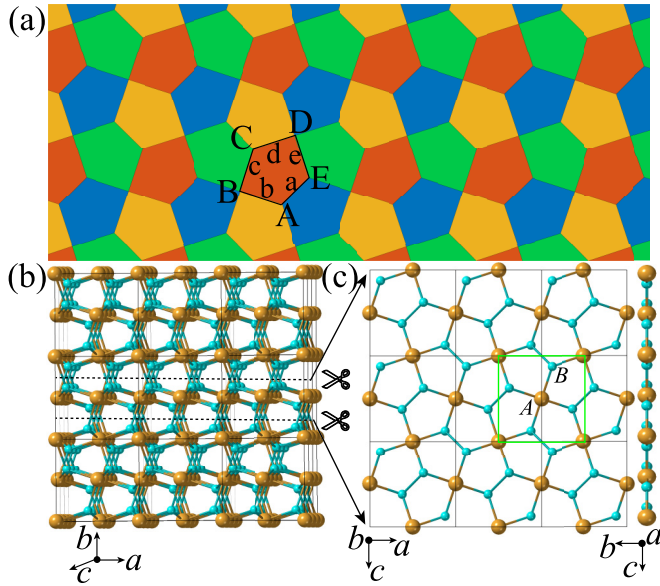


FIG. 1. (a) Illustration of the Cairo tessellation formed by type 2 pentagons tiling the plane. The angles and side lengths of a type 2 pentagon are shown. (b) Side view of a $3 \times 3 \times 3$ supercell of bulk AB_2 with the pyrite structure. (c) Left: Top view of single-layer AB_2 extracted from the bulk. Right: Side view of single-layer PtP_2 after DFT geometry optimizations, adopting the Cairo tessellation. The solid green lines enclose a unit cell of single-layer PtP_2 for the calculations.

of 1.3 eV [12]. There are a growing list of single-layer pentagonal materials such as AgN_3 [13,14], SiC_2 [15], CN_2 [16], and B_2C [17] recently predicted with the buckled Cairo tessellation. Notably, Yang *et al.* first reported that single-layer PtN_2 exhibits the ideal Cairo tessellation with completely coplanar Pt and N atoms [18].

We believe the above list of single-layer materials with the Cairo tessellation is incomplete. One question naturally arises: How can we search for single-layer materials with the Cairo tessellation? To find the answer to this question, we noticed that the nature has already had abundant compounds—especially the ones with the pyrite structure—where the Cairo tessellation is lurking. The pyrite structure possessed by FeS_2 is cubic with the general chemical formula AB_2 and space group $pa\bar{3}$ (No. 205). A side view of the pyrite structure is displayed in Fig. 1(b), showing that atomic layers containing A and B atoms stack along the b direction. The top view of each AB_2 layer is shown in Fig. 1(c), revealing the hidden Cairo tessellation. We assume that obtaining single-layer AB_2 with the Cairo tessellation is analogous to cutting the bonds between layers.

In this work we select A and B to be Pt and P, respectively, as Pt-P compounds are not common materials and also as P and N belong to the same group in the periodic table—the resulting single-layer structures should bear some similarity. According to the Materials Project [19], Pt and P can form only two stoichiometric compounds: PtP_2 and Pt_2P_5 , both of which are the intermediate phases in Pt-P molten glasses [20]. Little research has been performed on these two compounds. Thomassen first determined the crystal structure of PtP_2 as the

pyrite structure [21]. Further work by Baghdadi and Schmidt *et al.* led to the accurate measurement of the structure of a single crystal using a tin flux [22,23]. We use this somewhat uncommon compound as an example of exploring the hidden Cairo tessellation in the pyrite structure to discover novel single-layer PtP_2 using DFT calculations.

II. METHODS

We use the Vienna *ab initio* simulation package (VASP, version 5.4.4) for all of the DFT calculations [24]. We also use both the Perdew-Burke-Ernzerhof (PBE) and HSE06 hybrid density functionals [25,26] to approximate the exchange-correlation interactions. The electron-ion interactions are described by the PBE version of the potential data set generated from the projector-augmented wave (PAW) method [27,28]. These potentials treat $5d^9 6s^1$ states of Pt atoms and $3s^2 3p^3$ states of P atoms as valence electrons. We adopt a surface slab model to simulate single-layer PtP_2 . Each surface slab has a vacuum spacing of 18.0 Å that is sufficiently large to separate the image interactions. We use the plane waves with their kinetic cutoff energy below 550 eV for approximating the total electron wave function. Moreover, we use Γ -centered $12 \times 12 \times 12$ and $12 \times 12 \times 1$ k -point grids for the integration in the reciprocal space for bulk and single-layer PtP_2 , respectively [29]. For the HSE06 calculations on bulk PtP_2 , we use a $8 \times 8 \times 8$ k -point grid to reduce the computational time. We also decrease the k -point grid size for the calculations on single-layer PtP_2 to $8 \times 8 \times 1$ considering the spin-orbit coupling (SOC). All the HSE06 and SOC calculations are based on the optimized PBE structure.

We apply two methods to create an initial unit cell of single-layer PtP_2 for further geometry optimizations. In the first method (M1) we carve out a single-layer PtP_2 from its bulk structure. This initial structure is a buckled structure with noncoplanar Pt and P atoms. The second method (M2) is based on the first one, but we set all the atomic coordinates to be coplanar. By using these two methods, we expect to find two structures with local energy minima. The unit cells used in both methods consist of two formula units. VASP fully optimizes the in-plane lattice constants and atomic positions of the two unit cells of single-layer PtP_2 until the threshold (0.01 eV/Å) of interatomic forces is reached. At each step of the geometry optimizations, we set the total energy convergence to 10^{-6} eV.

We employ Phonopy [30] and VASP to obtain the phonon spectrum of single-layer PtP_2 following three steps. First, we use Phonopy to generate $3 \times 3 \times 1$ supercells. Next, we use VASP to calculate the interatomic forces for each supercell using a $4 \times 4 \times 1$ k -point grid. Finally, the forces are collected and post-processed by Phonopy to compute phonon frequencies at each wave vector along a high-symmetry k -point path.

III. RESULTS AND DISCUSSION

We begin with computing the lattice constant and the formation energy E_f^{bulk} of bulk PtP_2 . E_f^{bulk} is calculated as the difference between the total energy of bulk PtP_2 with reference to the energies of face-centered cubic Pt and monoclinic P. The calculated lattice constant and E_f^{bulk} are

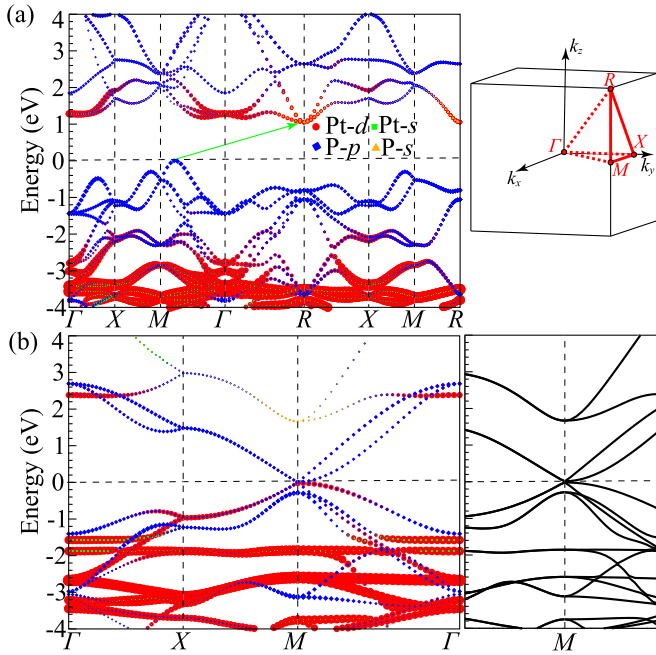


FIG. 2. (a) Calculated orbital-resolved band structure of bulk PtP₂. The first Brillouin zone and high-symmetry k -point paths are shown in the right side panel. The green arrow is used to aid the view of the indirect band gap. (b) Orbital-resolved band structure of single-layer PtP₂ with the Cairo tessellation. The bands are color coded by the contributions from Pt- d (red circle), Pt- s (green square), P- p (blue diamond), and P- s (brown triangle) orbitals. The larger symbol size corresponds to stronger contributions to a band. The right side panel shows the zoomed in band structure near the M point. The valence band maximum in (a) is set to zero.

5.75 Å and -697 meV/atom, respectively, both agreeing well with previous results (5.76 Å and -692 meV/atom, respectively) of DFT calculations recorded in the Materials Project (Materials Project id: mp-730) [19].

We next calculate the band structure of bulk PtP₂. Figure 2(a) shows the theoretical orbital-resolved band structure of bulk PtP₂ computed with the PBE functional. Consistent again with the band gap (1.02 eV) documented in the Materials Project [19], our calculated band structure shows that bulk PtP₂ is a semiconductor with an indirect PBE band gap of 1.06 eV. The valence band maximum (VBM) is located at a k point between the M and Γ points, and the conduction band minimum (CBM) occurs at the R point. The d orbitals of Pt atoms dominate the VBM, and the CBM originates from the contributions of d orbitals of Pt and s orbitals of P atoms. Because the PBE functional leads to underestimated band gaps [31], we further use the HSE06 hybrid density functional to correct the band gap. We find the corrected band gap using the HSE06 functional is 1.59 eV, which is within the visible light spectrum, so bulk PtP₂ may be useful for solar-energy conversion applications.

Having calculated the properties of bulk PtP₂, we set to focus on single-layer PtP₂. We mentioned in the Method section that we use two different initial geometries to obtain the stable structure of single-layer PtP₂. In the M1 method, the initial out-of-plane distance d —between the

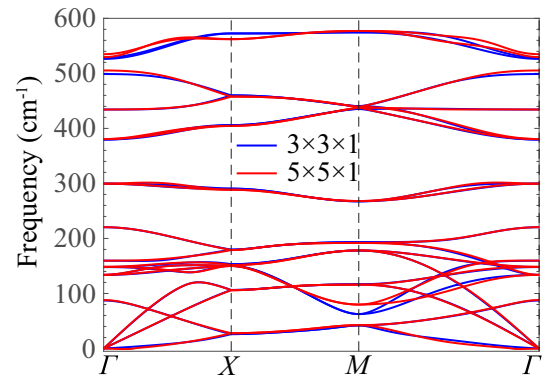


FIG. 3. Predicted phonon spectrum of single-layer PtP₂ with the Cairo tessellation calculated at the DFT-PBE level of theory. Two supercell sizes ($3 \times 3 \times 1$ and $5 \times 5 \times 1$) are used.

subplanes of Pt and P atoms—is 0.63 Å determined by the bulk pyrite structure. But the geometry optimization transforms the structure into a nearly completely planar structure with a negligible d of 0.003 Å. In this method the cross section of the surface slab also becomes slightly off a square. In the M2 method, the resulting structure is entirely planar and the cross section is strictly a square. The energy of the resulting structure from the M2 method is almost the same as that from the M1 method, but is trivially smaller by 0.1 meV per formula unit. We therefore conclude that single-layer PtP₂ prefers adopting a fully planar structure.

Figure 1(c) illustrates the side view of single-layer PtP₂ with the optimized, planar structure. The symmetry analysis performed by Phonopy shows that the space group of single-layer PtP₂ is $P4/mbm$ (No. 127), corresponding to a lower symmetry than bulk PtP₂. As a result of the structure flattening, the calculated in-plane lattice constant (5.83 Å) is slightly larger than that (5.75 Å) of bulk PtP₂. To confirm that the single-layer PtP₂ with the planar, pentagonal structure is dynamically stable, we calculate the phonon spectrum, which is shown in Fig. 3. The absence of imaginary phonon modes corroborates the dynamical stability. We also increase the supercell size for phonon calculations from $3 \times 3 \times 1$ to $5 \times 5 \times 1$, the resulting phonon spectrum is shown in Fig. 3. We observe the two phonon spectra are nearly identical, showing the convergence of the phonon spectra with respect to supercell sizes. Both phonon spectra conclude the dynamical stability of single-layer PtP₂ with the Cairo tessellation.

We then compare the geometry of a pentagon in the optimized single-layer PtP₂ structure to a type 2 pentagon illustrated in Fig. 1(a). We calculate the optimized, nearest-neighbor Pt-P and P-P bond length as 2.30 and 2.08 Å, respectively, corresponding to one constraint ($b = c = d = e$) of the special type 2 pentagon. The P-P-Pt, Pt-Pt-P, Pt-P-Pt bond angles are $A = E = 116.4^\circ$, $B = D = 90^\circ$, and $C = 127.2^\circ$, respectively. All of these side lengths and angles satisfy the minimum geometry constraints imposed on type 2 pentagon, i.e., $c = e$ and $B + D = 180^\circ$. Such a pentagonal geometry confirms that single-layer PtP₂ exhibits the Cairo tessellation.

To rule out the possibility of Pt and P forming a hexagonal single-layer structure, we also compute the energies of

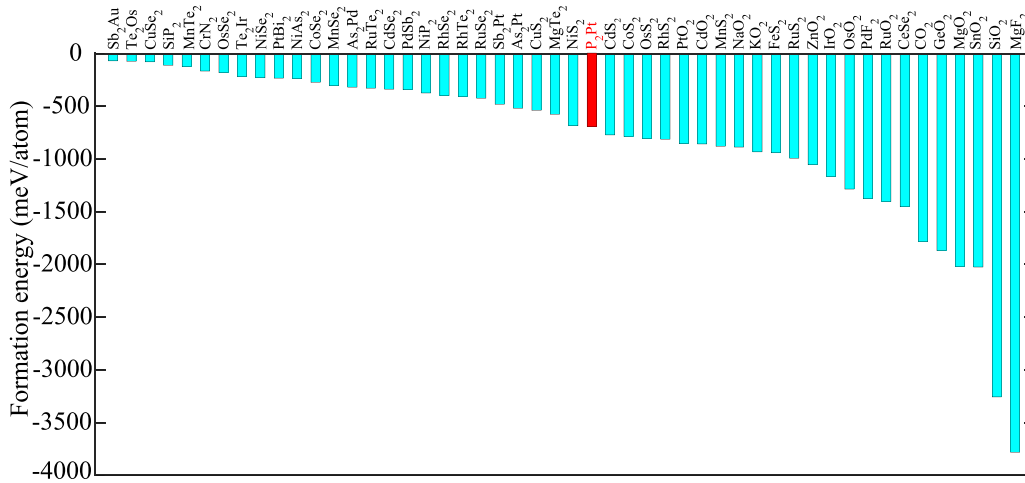


FIG. 4. Bulk formation energies from data mining the Materials Project [19] for the compounds with the pyrite structure, a general chemical formula AB_2 , and space group $pa\bar{3}$.

single-layer PtP_2 with the hexagonal trigonal prismatic ($2H$) and octahedral ($1T$) structures. We find that the energies of these two structures—both are found to be metallic—are higher than that of the pentagonal structure with the Cairo tessellation by 534 and 311 meV/atom, calculated with the PBE functional. The corresponding energy differences using the HSE06 functional are 682 and 397 meV/atom, respectively. Namely, the stability of single-layer PtP_2 with the three structures follows the order of stability from the highest to the lowest: Pentagonal $> 1T > 2H$. As such, the term single-layer PtP_2 henceforth refers to the the pentagonal structure with the Cairo tessellation.

We then calculate the formation energy E_f^{SL} of single-layer PtP_2 using the energy of its bulk counterpart as the reference [32]. We determine the E_f as 410 and 465 meV/atom, computed with the PBE and HSE06 functionals, respectively, which are somewhat large, excluding the feasibility of obtaining single-layer PtP_2 from bulk PtP_2 via the mechanical exfoliation method as used to obtain graphene [33]. A most viable method to obtain single-layer PtP_2 is therefore via a chemical method such as the chemical vapor decomposition.

We attempt to correlate the formation energies of bulk ($E_f^{bulk} = -697$ meV/atom) and single-layer PtP_2 ($E_f^{SL} = 410$ meV/atom). We use a simplified model assuming that the nearest neighboring Pt-P and P-P bonds contribute the most significantly to the formation energies. We count the number of Pt-P and P-P bonds in bulk PtP_2 as 24 and 4, respectively, for the 12 atoms in a unit cell. In other words, each bulk unit cell has 2 Pt-P and 1/3 P-P bonds per atom. Mathematically we write

$$E_f^{bulk} = 2E_{Pt-P} + 1/3E_{P-P}, \quad (1)$$

where E_{Pt-P} and E_{P-P} are the energies of the Pt-P and P-P bonds, respectively. Similarly, the six-atom unit cell of single-layer PtP_2 has eight Pt-P and two P-P bonds, corresponding to 4/3 Pt-P and 1/3 P-P bonds per atom. Therefore, we have

$$E_f^{SL} = 4/3E_{Pt-P} + 1/3E_{P-P}. \quad (2)$$

Taking the difference of Eqs. (1) and (2) gives

$$E_f^{SL} = E_f^{bulk} - 2/3E_{Pt-P}. \quad (3)$$

Equations (1) and (2) show that the number of P-P bonds remains the same when transforming from the bulk to single layer. Equation (3) shows that the energy cost for the dimension reduction is equivalent of removing 2/3 Pt-P bonds. Therefore, the Pt-P bond energy is calculated as 615 meV/atom. This oversimplified bond-counting model seems to indicate that the smaller the bulk formation energy (smaller E_f^{bulk}) of a compound with the pyrite structure, the less energy-consuming (smaller E_f^{SL}) to obtain a single-layer pentagonal structure.

Following the above argument, we perform a data-mining operation in the Materials Project to identify all of the compounds with the pyrite structure, a general chemical formula AB_2 , and space group $pa\bar{3}$. We find 50 such compounds with negative formation energies, implying they are stable in the bulk form. Figure 4 shows that the formation energies of these AB_2 compounds range widely from 69 meV/atom for $AuSb_2$ to 3780 meV/atom for MgF_2 . We expect that the compounds whose bulk formation energies lie in the left-hand side of the histogram correspond to small single-layer formation energies, enhancing the possibility of obtaining the single-layer form of these compounds. Interestingly, we notice that the simple bond-cutting model leads to nearly the same predicted pentagonal compounds (e.g., $MnTe_2$ and $OsTe_2$), which are also reported in the recently published Computational 2D Materials Database generated using a high-throughput approach with the structures of MnS_2 and PdS_2 as prototypes [34]. We leave the calculations of the single-layer formation energies and characterization of these compounds as future work.

We now focus on the electronic structure of single-layer PtP_2 . We first calculate the Bader charge transfer to understand the bonding characteristics of Pt-P and P-P bonds [35,36]. Here the Bader analysis is conducted on the all-electron density [37], i.e., the core electron density combined with the pseudovalence density. Consistent with the slightly more electronegativity of Pt than P (2.28 and 2.19 for Pt

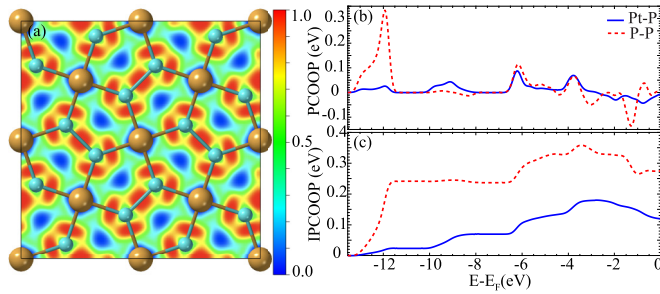


FIG. 5. (a) The electron localization function of single-layer PtP₂. (b) Projected and (c) integrated crystal orbital overlap population (PCOOP and ICOOP) of the Pt-P and P-P bonds in single-layer PtP₂.

and P, respectively, in the Pauling scale [38]), we find that 0.23 electrons are transferred from P to Pt in single-layer PtP₂, indicating the Pt-P bond is of the ionic nature. We next compute the electron localization functional (ELF) [39]. The calculated ELF of single-layer PtP₂ is shown in Fig. 5(a). We see that the ELF values near the P atoms are almost equal to 1.0, showing that the electrons are localized around the P atoms in the Pt-P bond indicative of ionic bonding. The ELF results also show the electrons are shared in the P-P bond, suggesting covalent bonding. Both the Bader charge analysis and ELF show that single-layer PtP₂ exhibits mixed types of ionic and covalent bonds. Furthermore, to provide a metric describing the strength of the Pt-P and P-P bonds, we calculate the crystal orbital overlap population (COOP) for the P-Pt and P-P bonds in a unit cell using the LOBSTER (local orbital basis suite towards electronic/structure reconstruction) tool [40]. Figure 5(b) shows the projected COOP (PCOOP) as a function of the electron energy. We observe that both the Pt-P and P-P bonds exhibit bonding and antibonding characteristics—represented by positive and negative PCOOP, respectively—below the Fermi level. The integrated COOP (ICOOP) is shown in Fig. 5(c). At the Fermi level, the ICOOP values for the Pt-P and P-P bonds are 0.12 and 0.27, respectively, showing that the P-P covalent bond is stronger than the ionic Pt-P bond.

Reducing bulk PtP₂ to single-layer nanosheets causes a drastic change in the band structure, as can be seen in Fig. 2(b). We observe a fourfold degeneracy of the conduction and valence bands at the *M* point, showing the metallic behavior of single-layer PtP₂. Similar to the bulk band structure, the *d* and *s* orbitals of Pt atoms and the *p* and *s* orbitals of P atoms all contribute to form the band structure of single-layer PtP₂. But the transition from a semiconducting bulk to a metallic single layer seems surprising to some extent. We mentioned that the PBE functional is well known to underestimate band gap, which may also lead to an incorrect conclusion that a semiconductor with a narrow band gap is considered to be metallic. We therefore use the more accurate HSE06 hybrid functional to calculate the density of states to confirm whether single-layer PtP₂ is truly metallic. Figure 6(a) shows the computed band structure using the HSE06 functional and the corresponding density of states is shown in Fig. 6(b). As can be seen, single-layer PtP₂ exhibits a direct band gap of 0.52 eV with the CBM and VBM both at the *M* point. Note that

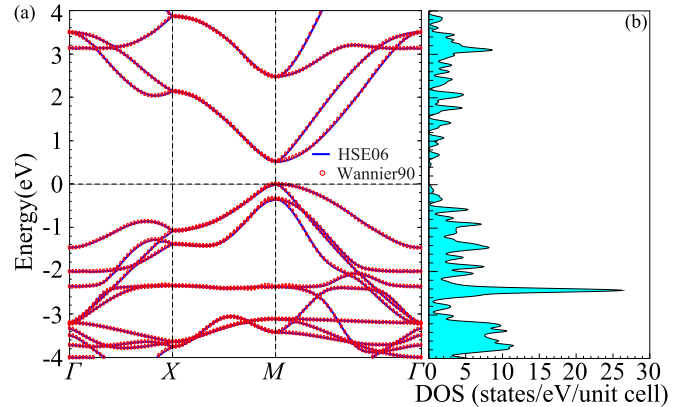


FIG. 6. (a) Band structure of single-layer PtP₂ calculated using the HSE06 functional and interpolated by the Wannier90 package. (b) Density of states (DOS) of single-layer PtP₂ calculated using the HSE06 functional. The valence band maximum is set to zero. The peaks in (b) result from the corresponding flat bands shown in (a), leading to the Von Hove singularities.

although the HSE06 functional is widely used and often leads to reasonable band gaps [41], the functional is not capable of discriminating between the different screening behavior for bulk and for 2D materials, more advanced approaches such as the optimally tuned screened range-separated hybrid (OT-SRSH) method [42] is called for in the future work to cross validate our HSE06 results. Although the band gap of single-layer PtP₂ is narrower than that of bulk PtP₂, semiconducting single-layer PtP₂ with a direct band gap may be useful in applications such as infrared detectors [43].

Reducing dimensions from three to two often leads to a widened band gap due to the quantum confinement effect. We actually also observe such effects in PtP₂. In particular, the band gap of bulk PtP₂ at the Γ point is increased from 2.71 to 3.78 eV for single-layer PtP₂ at the same *k* point. But the dimension reduction also causes a drastic symmetry change, leading to the degenerate bands at the *M* point. The interplay of quantum confinement and symmetry change results in an overall decrease in the band gaps from bulk to single-layer PtP₂.

Although single-layer pentagonal PtN₂ has been reported to exhibit a wider band gap (1.51 eV) than PtP₂ [18], the main concern is the stability of bulk PtN₂ with a positive formation energy. Namely, bulk PtN₂ decomposes into Pt and N₂ according to the Materials Project [19]. From the energetics point of view, if a bulk material is unstable, it is challenging to obtain the single-layer counterpart. By contrast, as shown in Fig. 4, bulk PtP₂ exhibits a negative formation energy and is a stable compound.

Several narrow-band-gap, single-layer semiconductors such as 1T' MoS₂ [44] and PbTe [45] have been predicted to be topological insulators, where the surface states behave as an insulator but the edge states show a spin-helical Dirac cone [46,47]. To examine the possible existence of such a topological phase in single-layer PtP₂, we study the edge states of single-layer PtP₂. We use tight-binding-like Wannier parameters and the iterative Green's function method [48,49] as implemented in the WannierTools package [50] to

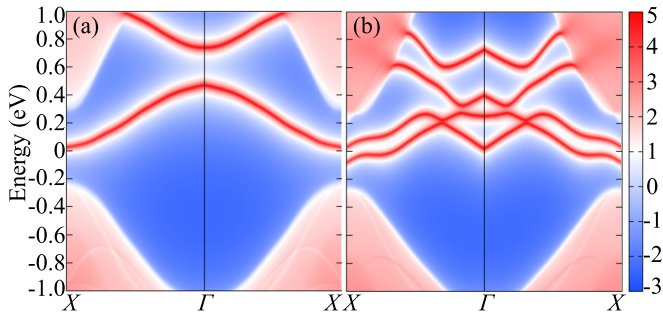


FIG. 7. Edge density of states of single-layer PtP₂ (a) without and (b) with spin-orbit coupling. The color intensity represents the magnitude of the edge spectrum function calculated via Green's function.

compute the edge states. According to the orbital-resolved band structure shown in Fig. 2(b), we use the Wannier90 package (version 1.2) to obtain 28 Wannier orbitals (s and d orbitals of two Pt atoms and s and p orbitals of four P atoms in a unit cell) projected from converged HSE06 wave functions in VASP calculations. Correspondingly, 56 Wannier orbitals are used if the spin-orbit coupling (SOC) is taken into account. As can be seen from Fig. 6, the obtained Wannier parameters are accurate enough to reproduce the HSE06 band structure. Without considering the SOC effect, we observe two degenerate edge density of states near the band gap as shown in Fig. 7(a). Including the SOC, the degeneracy is lifted,

doubling the number of edge density of states [see Fig. 7(b)]. But the spin-helical Dirac states remain absent, excluding single-layer PtP₂ as a topological insulator, possibly due to the weak SOC.

IV. CONCLUSIONS

In conclusion, we demonstrated an example of discovering 2D materials by uncovering the hidden Cairo tessellation in the pyrite structure. We predicted that single-layer PtP₂ is a new 2D material with a fully planar, pentagonal structure. We found that the PBE functional incorrectly predicted single-layer PtP₂ to be metallic. But the more accurate HSE06 hybrid density functional calculations showed that single-layer PtP₂ indeed exhibits a reduced, direct band gap in comparison with bulk PtP₂. A future work could be integrating the procedure of computational characterization followed in this work into a high-throughput framework for accelerating discovery of pentagonal 2D materials.

ACKNOWLEDGMENTS

We thank the start-up funds from Arizona State University. We also thank Dr. Jianfeng Wang, Dr. Bing Huang, and Dr. Xiaofeng Qian for helpful discussions. This research used computational resources of the Texas Advanced Computing Center under Contract No. TG-DMR170070.

- [1] K. S. Novoselov, A. K. Geim, S. V. Morozov, D. Jiang, Y. Zhang, S. V. Dubonos, I. V. Grigorieva, and A. A. Firsov, *Science* **306**, 666 (2004).
- [2] L. Song, L. Ci, H. Lu, P. B. Sorokin, C. Jin, J. Ni, A. G. Kvashnin, D. G. Kvashnin, J. Lou, B. I. Yakobson *et al.*, *Nano Lett.* **10**, 3209 (2010).
- [3] K. F. Mak, C. Lee, J. Hone, J. Shan, and T. F. Heinz, *Phys. Rev. Lett.* **105**, 136805 (2010).
- [4] B. Huang, G. Clark, E. Navarro-Moratalla, D. R. Klein, R. Cheng, K. L. Seyler, D. Zhong, E. Schmidgall, M. A. McGuire, D. H. Cobden *et al.*, *Nature (London)* **546**, 270 (2017).
- [5] H. L. Zhuang, M. D. Johannes, M. N. Blonsky, and R. G. Hennig, *Appl. Phys. Lett.* **104**, 022116 (2014).
- [6] C. Wang, X. Zhou, Y. Pan, J. Qiao, X. Kong, C.-C. Kaun, and W. Ji, *Phys. Rev. B* **97**, 245409 (2018).
- [7] D. Shechtman, I. Blech, D. Gratias, and J. W. Cahn, *Phys. Rev. Lett.* **53**, 1951 (1984).
- [8] L. Liu, I. Kankam, and H. L. Zhuang, *Comput. Mater. Sci.* **154**, 37 (2018).
- [9] L. Liu, I. Kankam, and H. L. Zhuang, [arXiv:1808.03409](https://arxiv.org/abs/1808.03409).
- [10] M. Rao, [arXiv:1708.00274](https://arxiv.org/abs/1708.00274).
- [11] D. Wells, *The Penguin Dictionary of Curious and Interesting Geometry* (Penguin, London, 1991).
- [12] A. D. Oyedele, S. Yang, L. Liang, A. A. Puretzy, K. Wang, J. Zhang, P. Yu, P. R. Pudasaini, A. W. Ghosh, Z. Liu *et al.*, *J. Am. Chem. Soc.* **139**, 14090 (2017).
- [13] C. L. Schmidt, R. Dinnebier, U. Wedig, and M. Jansen, *Inorg. Chem.* **46**, 907 (2007).
- [14] M. Yagmurcukardes, H. Sahin, J. Kang, E. Torun, F. Peeters, and R. Senger, *J. Appl. Phys.* **118**, 104303 (2015).
- [15] A. Lopez-Bezanilla and P. B. Littlewood, *J. Phys. Chem. C* **119**, 19469 (2015).
- [16] S. Zhang, J. Zhou, Q. Wang, and P. Jena, *J. Phys. Chem. C* **120**, 3993 (2016).
- [17] F. Li, K. Tu, H. Zhang, and Z. Chen, *Phys. Chem. Chem. Phys.* **17**, 24151 (2015).
- [18] Z. Liu, H. Wang, J. Sun, R. Sun, Z. F. Wang, and J. Yang, *Nanoscale* **10**, 16169 (2018).
- [19] A. Jain, S. P. Ong, G. Hautier, W. Chen, W. D. Richards, S. Dacek, S. Cholia, D. Gunter, D. Skinner, G. Ceder, and K. A. Persson, *APL Mater.* **1**, 011002 (2013).
- [20] E. Dahl, *Acta Chem. Scand* **21**, 1131 (1967).
- [21] L. Thomassen, *Z. Phys. Chem. B* **4**, 277 (1929).
- [22] A. Baghdadi, A. Finley, P. Russo, R. Arnott, and A. Wold, *J. Less-Common Met.* **34**, 31 (1974).
- [23] T. Schmidt, H. D. Lutz, and W. Hönl, *Z. Kristallogr. Crystal. Mater.* **190**, 143 (1990).
- [24] G. Kresse and J. Furthmüller, *Phys. Rev. B* **54**, 11169 (1996).
- [25] J. P. Perdew, K. Burke, and M. Ernzerhof, *Phys. Rev. Lett.* **77**, 3865 (1996).
- [26] A. V. Krukau, O. A. Vydrov, A. F. Izmaylov, and G. E. Scuseria, *J. Chem. Phys.* **125**, 224106 (2006).
- [27] P. E. Blöchl, *Phys. Rev. B* **50**, 17953 (1994).
- [28] G. Kresse and D. Joubert, *Phys. Rev. B* **59**, 1758 (1999).
- [29] H. J. Monkhorst and J. D. Pack, *Phys. Rev. B* **13**, 5188 (1976).
- [30] A. Togo and I. Tanaka, *Scr. Mater.* **108**, 1 (2015).
- [31] J. P. Perdew and M. Levy, *Phys. Rev. Lett.* **51**, 1884 (1983).

- [32] H. L. Zhuang and R. G. Hennig, *Jom* **66**, 366 (2014).
- [33] A. K. Singh, K. Mathew, H. L. Zhuang, and R. G. Hennig, *J. Phys. Chem. Lett.* **6**, 1087 (2015).
- [34] S. Hastrup, M. Strange, M. Pandey, T. Deilmann, P. S. Schmidt, N. F. Hinsche, M. N. Gjerding, D. Torelli, P. M. Larsen, A. C. Riis-Jensen, J. Gath, K. W. Jacobsen, J. J. Mortensen, T. Olsen, and K. S. Thygesen, *2D Mater.* **5**, 042002 (2018).
- [35] G. Henkelman, A. Arnaldsson, and H. Jónsson, *Comput. Mater. Sci.* **36**, 354 (2006).
- [36] W. Tang, E. Sanville, and G. Henkelman, *J. Phys.: Condens. Matter* **21**, 084204 (2009).
- [37] E. Aubert, S. Lebegue, M. Marsman, T. T. T. Bui, C. Jelsch, S. Dahaoui, E. Espinosa, and J. G. Ángyán, *J. Phys. Chem. A* **115**, 14484 (2011).
- [38] L. Pauling, *The Nature of the Chemical Bond and the Structure of Molecules and Crystals: An Introduction to Modern Structural Chemistry*, George Fisher Baker non-resident lectureship in chemistry at Cornell University (Cornell University Press, Ithaca, NY, 1945).
- [39] A. D. Becke and K. E. Edgecombe, *J. Chem. Phys.* **92**, 5397 (1990).
- [40] S. Maintz, V. L. Deringer, A. L. Tchougréeff, and R. Dronskowski, *J. Comput. Chem.* **37**, 1030 (2016).
- [41] A. J. Garza and G. E. Scuseria, *J. Phys. Chem. Lett.* **7**, 4165 (2016).
- [42] D. Lüftner, S. Refaely-Abramson, M. Pachler, R. Resel, M. G. Ramsey, L. Kronik, and P. Puschnig, *Phys. Rev. B* **90**, 075204 (2014).
- [43] T. McGill and D. Collins, *Semicond. Sci. Technol.* **8**, S1 (1993).
- [44] X. Qian, J. Liu, L. Fu, and J. Li, *Science* **346**, 1344 (2014).
- [45] J. Liu, X. Qian, and L. Fu, *Nano Lett.* **15**, 2657 (2015).
- [46] M. Z. Hasan and C. L. Kane, *Rev. Mod. Phys.* **82**, 3045 (2010).
- [47] X.-L. Qi and S.-C. Zhang, *Rev. Mod. Phys.* **83**, 1057 (2011).
- [48] F. Guinea, C. Tejedor, F. Flores, and E. Louis, *Phys. Rev. B* **28**, 4397 (1983).
- [49] M. L. Sancho, J. L. Sancho, and J. Rubio, *J. Phys. F* **14**, 1205 (1984).
- [50] Q. Wu, S. Zhang, H.-F. Song, M. Troyer, and A. A. Soluyanov, *Comput. Phys. Commun.* **224**, 405 (2018).